BIOCHEMISTRY
including biophysical chemistry & molecular biology

Article

pubs.acs.org/biochemistry

Molecular Origin of Electron Paramagnetic Resonance Line Shapes on β-Barrel Membrane Proteins: The Local Solvation Environment Modulates Spin-Label Configuration

Daniel M. Freed,[†] Ali K. Khan,[†] Peter S. Horanyi,[‡] and David S. Cafiso*,[†]

[†]Department of Chemistry and [‡]Department of Molecular Physiology and Biological Physics and Center for Membrane Biology, University of Virginia, Charlottesville, Virginia 22904-4319, United States

ABSTRACT: In this work, electron paramagnetic resonance (EPR) spectroscopy and X-ray crystallography were used to examine the origins of EPR line shapes from spin-labels at the protein−lipid interface on the β-barrel membrane protein BtuB. Two atomic-resolution structures were obtained for the methanethiosulfonate spin-label derivatized to cysteines on the membrane-facing surface of BtuB. At one of these sites, position 156, the label side chain resides in a pocket formed by neighboring residues; however, it extends from the protein surface and yields a single-component EPR spectrum in the crystal that results primarily from fast rotation about the fourth and fifth bonds linking the spin-label to the protein backbone. In lipid bilayers, site 156 yields a multicomponent spectrum resulting from different rotameric states of the labeled side chain. Moreover, changes in the lipid environment, such as variations in bilayer thickness, modulate the EPR spectrum by modulating label rotamer populations. At a second site, position 371, the labeled side chain interacts with a pocket on the protein surface, leading to a highly immobilized single-component EPR spectrum that is not sensitive to hydrocarbon thickness. This spectrum is similar to that seen at other sites that are deep in the hydrocarbon, such as position 170. This work indicates that the rotameric states of spin-labels on exposed hydrocarbon sites are sensitive to the environment at the protein−hydrocarbon interface, and that this environment may modulate weak interactions between the labeled side chain and the protein surface. In the case of BtuB, lipid acyl chain packing is not symmetric around the β-barrel, and EPR spectra from labeled hydrocarbon-facing sites in BtuB may reflect this asymmetry. In addition to facilitating the interpretation of EPR spectra of membrane proteins, these results have important implications for the use of long-range distance restraints in protein structure refinement that are obtained from spin-labels.

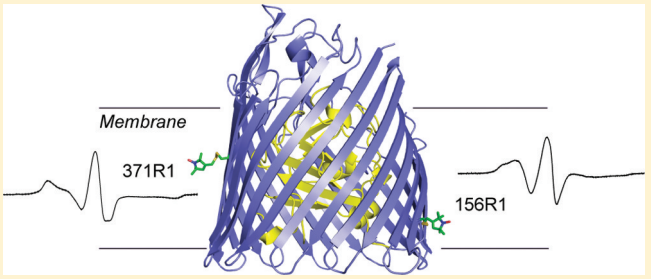

Spin-labels have proven to be powerful tools for probing protein structure and dynamics. In the EPR-based technique site-directed spin-labeling (SDSL), a spin-labeled side chain is used to probe the local structure and dynamics at the labeled site and to provide distance restraints between pairs of labeled side chains.[1−5] This approach is particularly valuable in the case of large protein complexes or membrane proteins, where other approaches may have limited utility. Spin-labels have also been used extensively to refine structures using high-resolution nuclear magnetic resonance, where paramagnetic enhancements of nuclear relaxation provide long-range distance restraints between nuclei and spin-labeled side chains.[6,7] Although there are several approaches that can be used to covalently attach spin-labels to proteins, the ease of attachment of labels based upon cysteine chemistry has made the methanethiosulfonate-derivatized cysteine side chain, R1, the most popular spin-labeled side chain for protein labeling (Figure 1a).

An important aspect of interpreting EPR spectra and long-range distances from spin-labeled sites is knowledge of the configuration of the label side chain. The configuration of the R1 side chain at labeled sites has been determined experimentally by examining the modes of motion that modulate the EPR spectrum,[8,9] and by crystallography on model proteins such as T4 lysozyme.[10−13] These studies have largely examined aqueous-exposed helical sites, where the internal motion of the label is dominated by dynamics about the fourth and fifth dihedral angles that link the label to the protein backbone (see Figure 1a). Label motion at these sites is not strongly influenced by neighboring residues, and differences in EPR spectra at such sites largely reflect differences in protein backbone dynamics on the nanosecond time scale.[8,14] Moreover, the preferred rotameric states of the side chain are strongly influenced by a weak interaction between the distal sulfur atom and the C_α proton.

Information about the motion and configuration of the spin-label at hydrocarbon-exposed sites in membrane proteins is more limited. Two structures were recently reported for the R1 side chain at helix surface sites in LeuT,[15] and this study suggests that unlike soluble proteins, the label R1 at hydrocarbon sites tends to make interactions with the protein

Received: June 24, 2011
Revised: September 2, 2011
Published: September 6, 2011

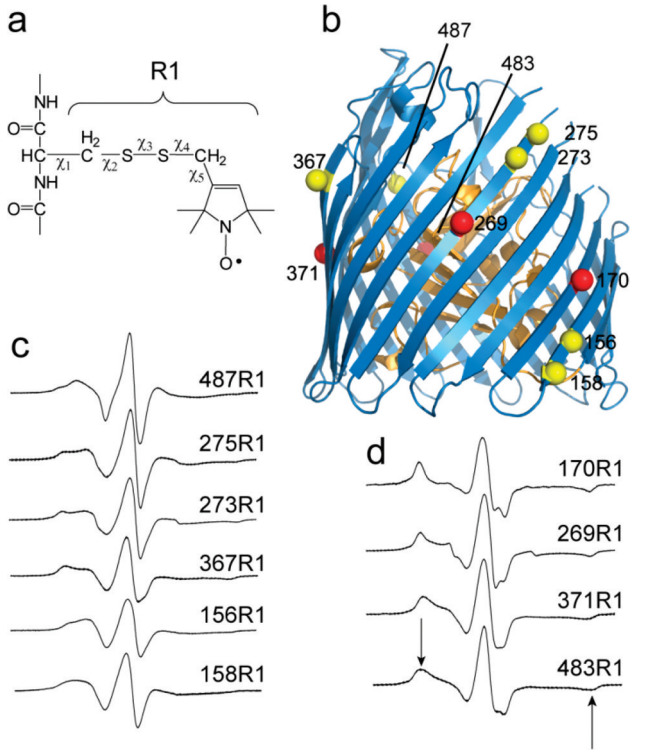

Figure 1. (a) Model for the spin-labeled side chain R1 obtained by derivatization with an MTSL spin-label. Five rotatable bonds link the R1 spin-label to the protein backbone, but motions that average the nitroxide magnetic interactions are often dominated by motion about χ_4 and χ_5 (see the text). (b) Model of BtuB (PDB entry 1NQH[24]) showing the position of 10 C_α atoms that have been spin-labeled with side chain R1. Previous work[19] indicates that when reconstituted into POPC bilayers, sites near the aqueous solvent interface (c) tend to yield EPR spectra that are multicomponent (yellow spheres) but at sites in the membrane interior (d) yield EPR spectra that are near the rigid limit (red spheres). All spectra are 100 G scans and normalized to equivalent spin numbers, except amplitudes of the spectra in panel d are scaled by a factor of 1.5. The arrows in panel d indicate the positions of the hyperfine extrema in the EPR spectrum, which are not averaged in rigid-limit EPR spectra.

surface. Until now, no structures of the R1 label at the surfaces of β-sheets in either membrane proteins or soluble proteins have been reported; however, the R1 environment should be more sterically restricted on the surface of a β-sheet than the surface of a helix. Work on the soluble β-sheet cellular retinol-binding protein[16] using mutagenesis coupled with SDSL demonstrated that R1 motion is strongly affected by the identity of nearest-neighbor residues and that highly ordered states result from β-branched residues such as valine and isoleucine at the non-hydrogen-bonded neighbor position. In the case of the β-barrel membrane protein BtuB (Figure 1b), the spectra are also modulated by the neighboring residues;[17] however, there is no consistent pattern of label motion and EPR line shape that can be correlated with the local steric environment. For example, the EPR spectrum of BtuB W371R1 is near the rigid limit on the X-band time scale, yet its nearest-neighbor residues consist of two threonines, one alanine, and one glycine. In contrast, the EPR line shape of BtuB Y275R1 results from R1 having an intermediate rate of motion, yet its nearest-neighbor residues consist of two lysines, one tyrosine, and one leucine. Moreover, the EPR spectra at some sites in BtuB are strongly influenced by lipid acyl chain length, an observation that suggests that protein backbone dynamics or protein shape might be modulated by membrane thickness.[17]

In this work, we determine the crystal structures for two spin-labeled sites on the hydrocarbon-facing surface of BtuB and examine the motion of the spin-labeled side chain, R1, as a function of the neighboring side chains and as a function of the local hydrocarbon environment. Labels at the β-barrel surface of BtuB do not assume the same rotameric states that are typically seen on solvent-exposed helical sites, and their motion is strongly influenced by interactions that are made with the protein surface. At position 156 in BtuB, which lies close to the solvent interface, two motional components are present in the EPR spectrum, which are a result of exchange between rotameric label states. In addition, the equilibrium between these states is strongly modulated by lipid environment. At position 170, which is in the bilayer interior, the EPR spectrum indicates that the spin-label is immobilized, and this immobilization is independent of lipid environment and neighboring residue identity. The W371R1 crystal structure suggests that immobilization at sites in the bilayer interior is due to interactions of the label with the protein surface. Collectively, the results indicate that label motion and its interactions with the protein surface are highly dependent upon solvation at the labeled site. These results are important for correctly interpreting line shapes of β-barrel membrane proteins, probing the environment at the protein−lipid interface, and determining structures and structural changes when spin-labels are used as long-range probes of interspin distances.

MATERIALS AND METHODS

Mutagenesis, Expression, Purification, and Spin-Labeling of BtuB Mutants. All mutations in BtuB were introduced into a pAG1 vector (for EPR spectroscopy) or a pET22b vector (for crystallization) using a QuickChange site-directed mutagenesis kit (Stratagene, La Jolla, CA), and the mutations were subsequently verified by nucleotide sequencing. For EPR spectroscopy of BtuB mutants, the expression, purification, spin-labeling, and reconstitution into lipid bilayers were performed following a procedure detailed previously.[18] All lipids were obtained from Avanti Polar Lipids (Alabaster, AL), and except where noted, all BtuB mutants were reconstituted into 1-palmitoyl-2-oleoyl-*sn*-glycero-3-phosphocholine (POPC) bilayers for EPR spectroscopy. POPC forms a fluid-phase bilayer over a broad temperature range, and as discussed elsewhere,[19] it has a hydrocarbon thickness that is similar to that of the native outer membrane of *Escherichia coli*. For BtuB crystallization, the expression, purification, and spin-labeling of BtuB were performed as described previously.[20,21]

Crystallization and Crystallographic Data Collection. Purified BtuB [11 mg/mL in 30 mM Tris (pH 8.0) and 20 mM C_8E_4] was crystallized by mixing 1 μL of BtuB and 1 μL of reservoir buffer in an EasyXtal hanging drop tray (Qiagen, Germantown, MD), containing 200 μL of total reservoir buffer for each crystallization condition, followed by incubation at 290 K. The reservoir buffer consisted of 200−550 mM magnesium acetate, 5.0−7.5% PEG3350, and 20 mM Bis Tris (pH 6.6). Crystals were visible after 1−2 days and grew to ~200 μm in the longest dimension after 1−2 weeks. For X-ray diffraction, BtuB crystals were transferred to cryo-buffer [150 mM magnesium acetate, 2.5% PEG3350, 20 mM Bis Tris (pH 6.6), 10 mM C_8E_4, and 20% glycerol] for 1−2 min before loop mounting and cryo-cooling by insertion into liquid nitrogen.

dx.doi.org/10.1021/bi200971x | *Biochemistry* 2011, 50, 8792−8803

Diffraction data were recorded at 90 K at the 22-ID and 22-BM beamlines at the Advanced Photon Source (Argonne National Laboratory, Argonne, IL).

Structure Determination. Indexing, integration, and scaling of the diffraction data were performed using HKL2000.[22] The structures were determined with the Phaser[23] maximum likelihood molecular replacement method, using PDB entry 1NQE[24] as a search model. To reduce model bias, the spin-labeled residues were deleted from the search model prior to molecular replacement. Model building was conducted in COOT;[25] unrestrained TLS[26] refinement was performed using Refmac,[27] and PHENIX [28] was used to refine the occupancy of the spin-label. The spin-labeled residues were manually built in COOT. Completed structures were evaluated and validated with MolProbity.[29]

EPR Spectroscopy of Spin-Labeled BtuB Mutants. Room-temperature (298 K) X-band EPR spectroscopy was performed on a Bruker EMX spectrometer equipped with a dielectric resonator (Bruker Biospin, Billerica, MA) or an E-line 102 Century series spectrometer from Varian outfitted with a loop gap resonator. Low-temperature (200 K) X-band EPR spectroscopy was performed with an E-line 102 Century series spectrometer from Varian equipped with a loop gap resonator. For all X-band measurements, 5 μL of an approximately 100 μM protein sample was loaded into Pyrex capillaries (0.60 mm inside diameter × 0.84 mm outside diameter, Fiber Optic Center, Inc., New Bedford, MA) using a syringe, and EPR spectroscopy on spin-labeled BtuB crystals was performed as described previously.[21] Low-temperature (200 K) Q-band EPR spectroscopy was performed on an ELEXSYS E-500 spectrometer equipped with an ER5106 QT-W resonator (Bruker Biospin) with 5 μL of approximately 100 μM protein samples loaded with a syringe into quartz capillaries (0.60 mm inside diameter × 0.84 mm outside diameter, Fiber Optic Center, Inc.). All EPR spectra were recorded with either a 100 G (at 298 K) or 150−200 G (at 200 K) magnetic field sweep at a 2.0 mW incident power. The phasing and normalization of EPR spectra were performed using LabVIEW provided by C. Altenbach (University of California, Los Angeles, CA).

Saturation Recovery EPR. Saturation recovery was performed on an X-band ELEXSYS E-580 spectrometer equipped with an MS-2 split-ring resonator (Bruker Biospin). The spectrometer was fitted with a Stanford Research Instruments (Sunnyvale, CA) SR445A amplifier in place of the video amplifier originally supplied with the instrument. For these measurements, 5 μL of an approximately 100 μM protein sample was loaded into Pyrex capillaries (0.60 mm inside diameter × 0.84 mm outside diameter, Fiber Optic Center, Inc.) using a syringe. A 500 ns saturating pump pulse was applied to the center of the $m_I = 0$ hyperfine line, and a 2 mW continuous wave (CW) observe power was applied at the same frequency. The field was stepped on- and off-resonance by 100 G at 5 Hz to subtract any background signal. Each measurement was independently repeated three times with good reproducibility (standard deviations within 75 ns), and the average T_1 relaxation times from the three measurements are reported.

Modeling of EPR Spectra. Low-temperature (200 K) X- and Q-band spectra were fit using an effective Hamiltonian rigid limit model executed in LabVIEW. From these fits, the hyperfine **A** and **g** tensor values were determined and used as constraints for fitting the room-temperature EPR spectra with the Microscopic Order Macroscopic Disorder (MOMD) model[30] implemented in the Multicomponent program developed by C. Altenbach. The following tensor values were used for spectral fitting: $g_{xx} = 2.0085$, $g_{yy} = 2.0059$, and $g_{zz} = 2.0021$; $A_{xx} = 6.5$, $A_{yy} = 5.6$, and $A_{zz} = 35.0$.

In the MOMD model, three coordinate frames are used to represent the microscopic motion of the nitroxide with respect to a fixed macroscopic director. In the molecule-fixed molecular frame (X_M, Y_M, and Z_M), Z_M is taken to lie along the 2p orbital of the nitroxide, X_M is coincident with the nitroxide bond axis, and Y_M is selected for a right-handed coordinate system. The molecular frame is the principal frame for the nitroxide hyperfine **A** and **g** tensors. The second coordinate frame is the rotational diffusion tensor frame (X_R, Y_R, and Z_R), which is related to the molecular frame by a $z-y-z$ Euler rotation using angles γ_D, β_D, and α_D, where a positive angle produces a counterclockwise rotation when viewed from the positive side of the rotating axis. The rate of nitroxide motion about each of these axes and their orientation with respect to the molecular frame indicate which R1 dihedrals are undergoing torsional oscillations that are contributing to motional averaging in the EPR spectrum. A restoring potential can be implemented that constrains the amplitude of diffusion about Z_R within a cone defined by the instantaneous angle θ between Z_R and the symmetry axis of the conical potential, which defines the z-axis of the third coordinate frame, the director frame. The director frame is fixed with respect to the protein and forms an angle ψ with respect to the external magnetic field. To obtain the final spectrum corresponding to an isotropic distribution of protein orientations, the spectra are summed over ψ.

The high degree of overlap between the fast and slow components in the 156R1 spectra introduces significant uncertainty into the fitting process. To address this issue, we initially fit the single-component 156R1 spectrum in DLPC bilayers and used the final parameters from this fit as initial input parameters for the fast component during the subsequent two-component fits. Additionally, because of the correlation between rotational diffusion and local order, the spectra were fit without a restoring potential to reduce fitting time and the number of parameters. In fact, better fits were obtained for the spectra presented here assuming anisotropic diffusion without a restoring potential, especially with respect to the high-field manifold.

During fitting, the **R** tensor (diffusion tensor in Cartesian representation) was allowed to vary for each component independently. Once a good fit to the central line was established, the Euler angles were adjusted for each component, paying special attention to the quality of fit at the high-field manifold. If necessary, the **R** tensors were varied again; this process was iteratively repeated until a satisfactory fit was obtained. In cases of simple z-axis anisotropic motion, only angles γ_D and β_D were varied to constrain the number of fitting parameters. Likewise, for simple x-axis anisotropic motion, only γ_D was varied. Subsequently, the Lorentzian (and, if necessary, Gaussian) line widths, initially set to 0 G, were allowed to vary to obtain the final fit. In some cases, the **A** tensor values were allowed to vary by 0.6 G if necessary to obtain the best fit. The quality of the fit was assessed using the reduced χ^2 between the experimental and theoretical spectra, as well as visually evaluating the match between prominent spectral features.

RESULTS

In this work, the *E. coli* outer membrane protein BtuB was used to examine the molecular basis of R1 spin-label motion at

hydrocarbon-exposed sites on β-barrel membrane proteins. Shown in Figure 1 are EPR spectra obtained for several sites on BtuB that have been labeled with the spin-label side chain R1[17,19] and reconstituted into POPC bilayers. The EPR spectra from the outer surface of BtuB are quite variable but can be divided into two general types: spectra that are clearly multicomponent indicating that R1 exhibits at least two types of motion (Figure 1c) and spectra that are dominated by a component due to a slowly moving nitroxide, where the hyperfine anisotropy is not averaged (Figure 1d). Although there are exceptions, the multicomponent spectra arise more frequently from residues in the aqueous phase or near the aqueous solvent interface, while the strongly immobilized spectra originate almost exclusively from spin-labeled sites buried in the membrane hydrocarbon.

Structural Model of T156R1 from X-ray Crystallography. T156R1 is at a site near the aqueous solvent interface that exhibits a multicomponent EPR spectrum (Figure 1c). To investigate the origin of these dynamic modes, we determined the structure of T156R1 at 90 K (Figure 2). The crystals of BtuB

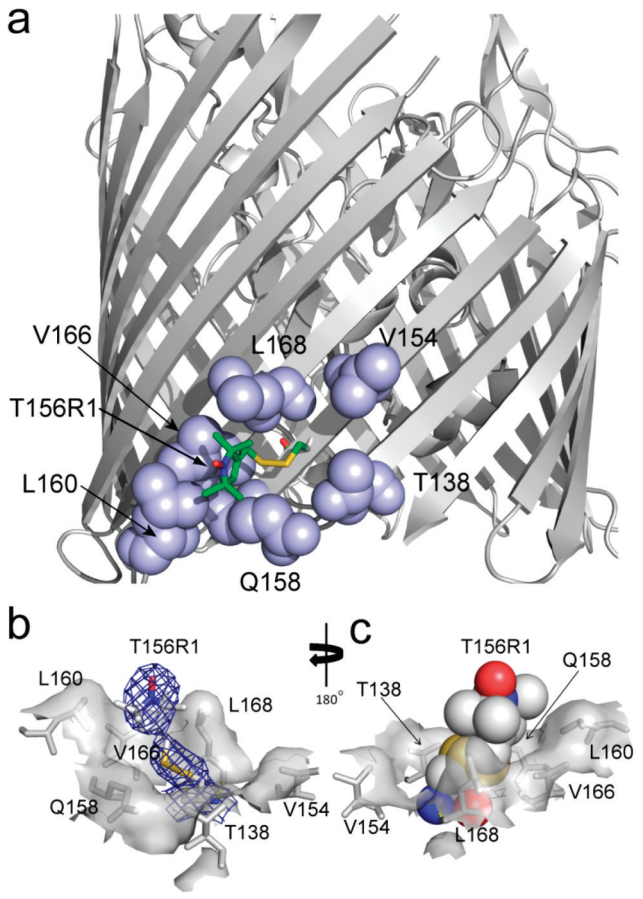

Figure 2. (a) X-ray crystal structure (90 K) of BtuB T156R1 (PDB entry 3RGM) determined at 2.6 Å showing the R1 side chain (as sticks) and the positions of the nearest-neighbor residues in a Corey, Pauling Koltun rendering. (b and c) Alternate views of the site around T156R1, with the van der Waals surface colored gray. In panel b, the $2F_o - F_c$ electron density is shown as blue mesh contoured at 1σ. Data collection and refinement statistics are listed in Table 1.

T156R1 diffracted to a resolution of 2.6 Å, and the resulting structure was refined to an R_{free} of 25.39%; the complete data collection and refinement statistics are listed in Table 1.

Table 1. X-ray Data Collection and Refinement Statistics for BtuB T156R1 and W371R1

	BtuB T156R1	BtuB W371R1
	Data Collection	
beamline	APS-22ID	APS-22BM
wavelength (Å)	1.000	1.000
temperature (K)	90	90
no. of reflections observed	224348	266642
no. of unique reflections	27492	37950
resolution range (Å)[a]	50−2.60 (2.64−2.60)	50−2.30 (2.38−2.30)
space group	$P3_121$	$P3_121$
cell dimensions	$a = b = 81.6$ Å, $c = 227.7$ Å	$a = b = 81.7$ Å, $c = 227.1$ Å
	$\alpha = \beta = 90°$, $\gamma = 120°$	$\alpha = \beta = 90°$, $\gamma = 120°$
R_{sym} (%)	6.2 (48.1)	10.5 (32.5)
redundancy	8.2	7.0
	Refinement	
resolution range (Å)	44.3−2.60 (2.67−2.60)	33.4−2.30 (2.36−2.30)
no. of reflections used	26070	35973
completeness (%)	98.3 (82.7)	95.2 (74.0)
R_{cryst} (%)[b]	21.32	22.16
R_{free} (%)[c]	25.39	24.98
rmsd		
bond lengths (Å)	0.020	0.023
bond angles (deg)	1.817	1.953
no. of atoms		
protein	4535	4612
water	86	130
other	C_8E_4 (6), Mg (11)	C_8E_4 (7), Mg (3)
PDB entry	3RGM	3RGN

[a]Data for the highest-resolution shell given in parentheses. [b]$R_{cryst} = \sum||F_{obs}| - |F_{calc}||/\sum|F_{obs}|$, where F_{obs} and F_{calc} are the observed and calculated structure factor amplitudes, respectively. [c]R_{free} is the R_{cryst} calculated using 5% of the data that are randomly chosen and omitted from the refinement.

Clear electron density is observed for the entire R1 side chain, allowing for determination of the χ_1−χ_5 dihedral angles (Table 2). The first two dihedral angles, χ_1 and χ_2, are in a

Table 2. Rotamer Designations and Summary of R1 Dihedral Angles

mutant	rotamer	χ_1	χ_2	χ_3	χ_4	χ_5
T156R1	{t,m}	176	−83	−94	−82	−30
W371R1	{p,p}	47	78	64	113	130

{t,m} rotamer using the conventions of Lovell et al.[31] This rotamer has been observed previously for R1 at solvent-exposed helical sites, but it is the least frequent of the three rotamers that are seen.[32] Because of the large absolute value of χ_2 (−83°), the S_δ−HC_α stabilizing interaction that is frequently seen in spin-labeled α-helical structures is absent (d = 4.2 Å). Instead, the R1 side chain appears to be stabilized by other interactions with the protein backbone, including S_δ−N_{i+1} and S_δ−O═C interactions (d = 3.5 Å). These interatomic distances are consistent with the other {t,m} rotamers reported in the literature[11,12] and may be important R1−backbone interactions that stabilize the spin-label in this configuration. In two recently

dx.doi.org/10.1021/bi200971x | Biochemistry 2011, 50, 8792−8803

published structures of R1 at hydrocarbon-exposed helical sites,[15] R1 assumes the {m,m} rotamer (the most common rotamer at helical sites) and is found to fold back onto the protein surface. In contrast, the 156R1 side chain projects away from the protein backbone where the nitroxide ring is localized in a hydrophobic pocket formed by the side chains of Q158, L160, V166, and L168.

The substitution of R1 at position 156 did not perturb BtuB structure. The all-atom pairwise rmsd compared to the wild-type apo structure[24] is 0.21 Å; however, small changes in the local side chain rotamer distribution are evident in neighboring residues. The largest change occurs for residue $i + 2$, Q158, where the first rotatable bond isomerizes moving the ε-nitrogen approximately 3 Å from its position in the wild-type protein (Figure 3). Compared to the wild-type structure, the L160 conformer is also altered in the spin-labeled structure as is the L168 side chain (Figure 3).

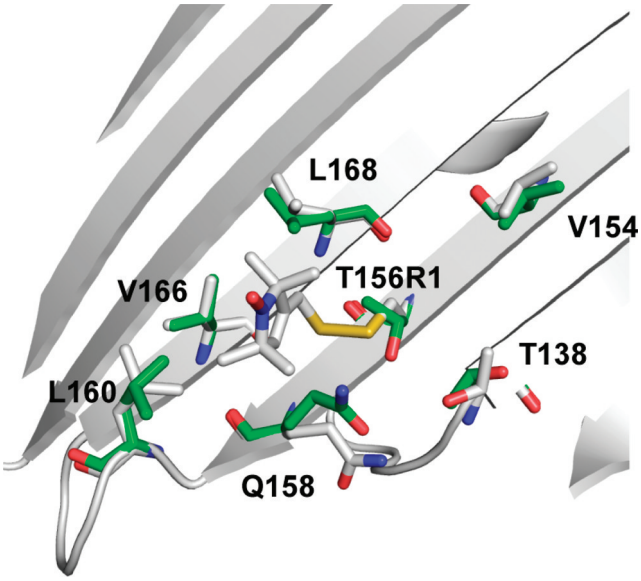

Figure 3. BtuB T156R1 crystal structure superposed on the wild-type coordinates (PDB entry 1NQE). T156R1 nearest-neighbor residues from the spin-labeled structure are rendered as sticks and colored gray, whereas the same residues from the wild-type structure are colored green. The Q158, L160, and L168 rotamers are altered upon introduction of R1 at position 156.

EPR Spectra and the Crystal Structure Suggest a Mode of Motion for T156R1. Shown in Figure 4 are EPR spectra of BtuB T156R1 reconstituted into POPC bilayers and in the protein crystal at room temperature. The POPC spectrum can be simulated using the MOMD model (see Materials and Methods) assuming that the spin-label undergoes two modes of motion: a relatively fast (1.7 ns) anisotropic motion about the z-axis of the diffusion tensor and a slower anisotropic x-axis motion (see Table 3). The room-temperature EPR spectrum obtained from *in surfo* crystals of BtuB T156R1 is different and can be simulated by a single component undergoing relatively fast z-axis motion (1.7 ns), similar to the fast component seen for the POPC sample. The EPR spectrum of BtuB T156R1 in crystallization buffer is identical to the crystalline spectrum, and lowering the temperature of this sample did not induce the appearance of a second slow component in the EPR spectrum, such as that seen in the POPC spectrum (data not shown). As a result, it is likely that

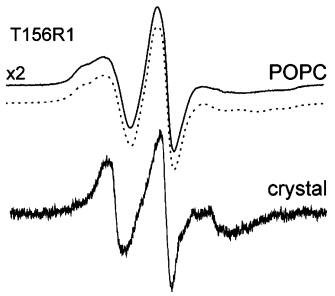

Figure 4. EPR spectra of BtuB T156R1 reconstituted into POPC bilayers (top) and a sample of ~20−30 intact protein crystals suspended in crystallization buffer (bottom). The dashed line represents the fit to the POPC spectrum (see Table 3 for the fit parameters). The room-temperature crystalline EPR spectrum consists of a single component undergoing fast rotational diffusion on the EPR time scale; the rate and anisotropy of the motion are similar to those of T156R1 in DLPC bilayers. All spectra are 100 G scans.

the label conformer observed in the crystal structure (the {t,m} rotamer) gives rise to the EPR spectrum of the crystal at room temperature (and the fast component seen in the POPC spectrum). This assignment is consistent with the MOMD fit. From this fit, the Euler angles for the fast component can be used to plot the rotational diffusion tensor frame onto the T156R1 crystal structure (Figure 5). In the context of this model, the orientation of the z-axis is roughly in a direction that would be the average of the direction for the fourth and fifth bonds linking the spin-label to the protein backbone, indicating that 156R1 is executing rapid rotation about the χ_4 and χ_5 bonds. Rotameric conversion about about χ_1−χ_3 is unlikely to be rapid on the EPR time scale, and motional averaging of the nitroxide magnetic interactions about χ_4 and χ_5 is consistent with previous studies of R1 in T4 lysozyme.[9]

Mutagenesis of Neighboring Residues Is Consistent with the Motional Model for T156R1. For β-sheet structures, a residue may interact with hydrogen-bonded (HB) and non-hydrogen-bonded (NHB) neighbors and with residues at positions $i \pm 2$. In general, these interactions are dependent on the side chain configuration and on the local strand twist and tilt.[33] To test the model presented in Figure 5, we obtained EPR spectra from mutagenesis of the side chains surrounding T156R1. The EPR spectra are shown in Figure 6, and the fits to the spectra using the MOMD model are listed in Table 3.

All the spectra shown in Figure 6 result from multiple motional components and require two modes of motion to be reasonably simulated by the MOMD model. In some cases, the line shapes of T156R1 are not strongly affected by mutation of the surrounding residues, although in many cases, these mutations shift the relative populations of the fast and slow components in the EPR spectrum of T156R1. Substitutions at the HB neighbor, L168, have the strongest effects, and increased steric size at this site increases the fraction of the slow component in the EPR spectrum. As seen in Figure 6 and Table 3, the L168W substitution produces a large change and inverts the populations to strongly favor the slow component. The larger side chain at position 168 is expected to sterically interfere with the position of T156R1 in the {t,m} rotamer and may force R1 to favor an alternate rotamer of χ_1 and/or χ_2 that yields the slow spectral component.

The $i + 2$ residue (Q158) lies close to the label disulfide, and as discussed above, Q158 is also the only residue that assumes a

Table 3. Dynamic Parameters from the MOMD Fits[a]

mutant	component	%	$\tau(x)$ (ns)	$\tau(y)$ (ns)	$\tau(z)$ (ns)	α	β	γ
T156R1 DLPC	2	100	–	11	1.7	−23	65	−26
T156R1 DMPC	1	22	4.3	–	–	0	0	11
	2	78	–	12	2.1	−23	63	−26
T156R1 POPC	1	26	14	–	–	0	0	17
	2	74	–	20	1.7	−24	58	−18
T156R1 DiErPC	1	59	7.6	–	–	0	0	31
	2	41	17	–	2.4	−36	50	−13
T156R1/T138A	1	27	6.9	–	–	0	0	20
	2	73	–	13	2.3	−28	63	−17
T156R1/T138Q	1	49	11	–	–	0	0	22
	2	51	–	18	1.7	−34	54	−11
T156R1/T138W	1	31	4.6	–	–	0	0	13
	2	69	–	–	1.1	0	65	−31
T156R1/L168A	1	21	6.1	–	–	0	0	28
	2	79	–	13	2.7	−23	65	−27
T156R1/L168V	1	33	9.0	–	–	0	0	23
	2	67	–	13	2.4	−28	62	−22
T156R1/L168W	1	65	7.8	–	–	0	0	34
	2	35	–	–	0.96	0	55	0
T156R1/V154A	1	52	3.1	–	–	0	0	20
	2	48	–	12	3.0	−29	65	−31
T156R1/V154Q	1	64	5.4	–	–	0	39	11
	2	36	–	–	0.56	0	54	−40
T156R1/Q158A	1	39	4.6	–	–	0	0	21
	2	61	4.7	–	16	52	37	−10
T156R1/Q158N	1	50	6.2	–	–	0	0	25
	2	50	8.4	–	5.4	45	45	−2
T156R1/L160A	1	35	8.0	–	–	0	0	24
	2	65	–	13	3.2	−31	62	−19

[a]The slow component is component 1, whereas the fast component is component 2. The slow component was fit with intermediate to slow x-axis anisotropic motion. In most cases, the majority of motional averaging in the fast spectral component was due to fast z-axis anisotropic motion. The dashes represent anisotropic correlation times from the fits that were slower than the time scale for averaging at X-band ($\tau > \sim 50$ ns). In these cases, to reduce the number of parameters, the correlation times were arbitrarily set to 167 ns ($R = 6.0$) for the remainder of the fit and thus are not reported.

significantly different rotamer in the T156R1 structure and the wild-type BtuB structures. Mutations at residue 158 affect the axes and rates of rotation for the fast component and the rates of motion for the slow component. Smaller side chains at position 158 result in faster motional rates for the slow component and slower diffusion about the z-axis for the fast component. Additionally, the fraction of label giving rise to a slow component increases for Q158N and Q158A compared to that of the wild-type residue.

As discussed below, the likely source of the slow component is an alternate label rotamer, which differs from that found in the crystal structure. We do not know the rotameric state that gives rise to the slow component in these EPR spectra, but the {t,t} rotamer is energetically reasonable[32] and would be allowed within the local side chain environment around T156R1. Moreover, in this configuration, R1 would interact more closely with T138 and Q158, which could account for effects of these mutations on the EPR line shapes of T156R1. The interaction between R1 and the non-hydrogen-bonded neighbor T138 is not strong in the {t,m} state, and while two mutations do not change the motion of the label, the T138Q mutation increases the population of the slow component. This is consistent with modeling of the {t,t} rotamer indicating that this rotamer might be favored with glutamine rather than threonine at position 138. Another possible alternate configuration is the commonly observed {m,m} rotamer, although modeling of this rotamer into the T156R1 crystal structure requires adjustment of T156R1 dihedrals other than just χ_1, and this rotamer would sterically clash with T138.

Bilayer Thickness Shifts Dynamic Modes of the BtuB T156R1 Spin-Label. Previous work demonstrated that the 156R1 EPR line shape was sensitive to hydrocarbon thickness.[17] Specifically, it was found that thinner membranes resulted in an increased level of motional averaging of 156R1, but that R1 motion was not strongly affected by the phase state of the surrounding lipid. It was proposed that R1 does not interact strongly with annular lipids but that it might report changes in the structure or dynamics of the β-barrel in response to a hydrophobic mismatch. Shown in Figure 7 are EPR spectra of T156R1 in lipid bilayers of four different thicknesses, all in the liquid crystalline state, as well as simulations of these spectra using the MOMD model (see Table 3 for parameters).

In DLPC bilayers, 156R1 is a single-component spectrum; the MOMD fits suggest that the spin-label is undergoing rapid oscillations about the χ_4 and χ_5 bonds (1.7 ns). This spectrum is identical to the crystalline 156R1 EPR spectrum, in which BtuB was crystallized from a C_8E_4 micellar solution. For the DMPC spectrum, this fast component is essentially unchanged, but an additional component having an intermediate motion (4.3 ns)

dx.doi.org/10.1021/bi200971x | Biochemistry 2011, 50, 8792–8803

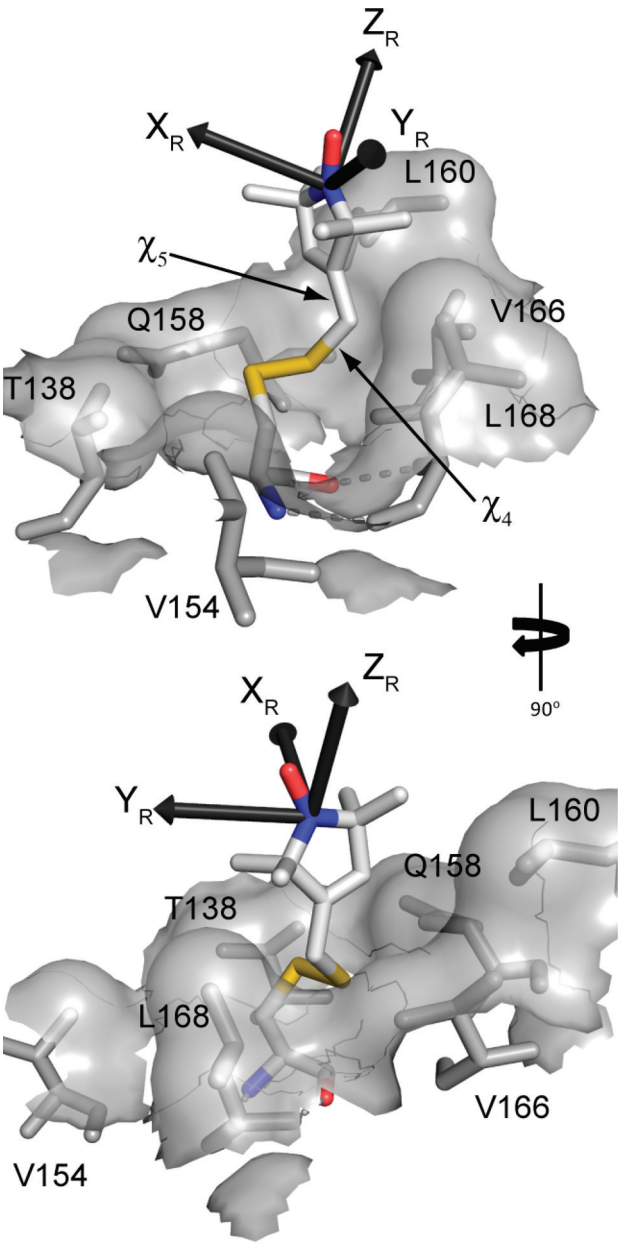

Figure 5. Rotational diffusion tensor frame for the fast component plotted onto the 156R1 crystal structure. From the correlation times determined from the MOMD fit (see Table 3), it is apparent that the label is executing rapid rotation about the χ_4 and χ_5 dihedrals.

about the x-axis of the molecular frame ($\gamma_D = 11$; $\beta_D = 0$) is present. With an increasing bilayer thickness, the population of the slow component increases and reaches 59% of the total spin population in DiErPC bilayers. Although no pattern can be seen in the rotational rates of the slow component as a function of bilayer thickness, the axes of rotation change slightly with thicker membranes. These results suggest that changes in membrane thickness primarily affect an equilibrium between two dynamic modes of T156R1, which appear to represent different rotameric states (see below). The fast correlation time $\tau(z)$ that makes the most significant contribution to the motional averaging of T156R1 remains essentially constant with membrane thickness, suggesting that membrane thickness does not affect line shape directly through changes in nanosecond backbone fluctuations as previously proposed.[17]

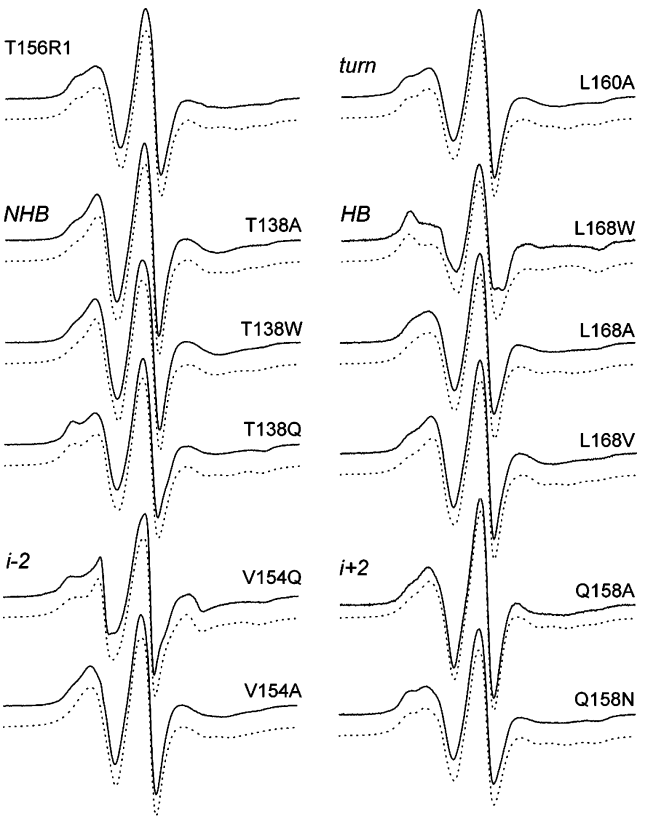

Figure 6. EPR spectra of BtuB T156R1 reconstituted into POPC vesicles and spectra from 11 mutants of T156R1, reconstituted into POPC bilayers, where the nearest-neighbor residues have been mutated. These spectra include those from mutations to the $i \pm 2$ residues (V154 and Q158), the hydrogen-bonded (L168) and non-hydrogen-bonded (T138) neighbors, and residue L160, which is on a periplasmic turn and forms the apex of a hydrophobic pocket near 156R1. The dashed lines below each spectrum represent the MOMD simulations for each spectrum (see Table 3 for the parameters used to generate each spectrum). All spectra are 100 G scans.

Structural Origins of the Slow Dynamic Mode of T156R1. Some R1 rotameric exchange processes, such as isomerization about the disulfide, are slow on the X-band EPR time scale ($\tau > \sim 50$ ns).[9] Slow rotameric exchange can produce multiple components in the continuous wave EPR spectrum, which are indistinguishable from protein conformational equilibria that are also slow on the X-band time scale. However, because protein conformational exchange is typically at least 1 order of magnitude slower than rotameric exchange and is also slow on the nitroxide T_1 relaxation time scale, T_1 measurements can be used to differentiate rotameric exchange from conformational exchange.[34]

To determine the origin of the multicomponent line shape, BtuB T156R1 was reconstituted into DLPC, POPC, and DiErPC bilayers and saturation recovery EPR was used to measure the T_1 relaxation time of each sample. As seen in Figure 8, each of the signals recovered to reach equilibrium with a single-exponential time course. The curves could be fit to the expression $M_z(t) = M_0(1 - e^{t/T_1})$, yielding a single-exponential fit and one apparent T_1 value. Because the T156R1 spectra in POPC and DiErPC have two motional components, the single-exponential recovery indicates that the rate of exchange between dynamic modes is fast on the T_1 time scale: $k_{ex}^{AB} \gg {}^1/_2(1/T_1^A - 1/T_1^B)$, where T_1^A and T_1^B represent

dx.doi.org/10.1021/bi200971x | Biochemistry 2011, 50, 8792–8803

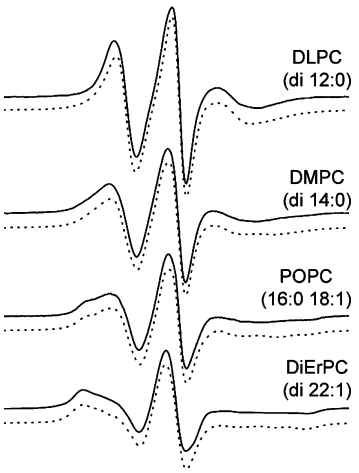

Figure 7. Comparison of T156R1 EPR spectra at 25 °C that are reconstituted into lipid bilayers of increasing hydrocarbon thickness. The hydrocarbon thicknesses, determined previously,[40,41] are approximately 19.5, 25.0, 27.1, and 43.4 nm for DLPC, DMPC, POPC, and DiErPC, respectively. The EPR line shapes are shown as solid traces, and the MOMD fits are shown as dashed lines below each spectrum. The DLPC spectrum could be fit with a single component, and the population of a second slow component increases with bilayer thickness (see Table 3 for the MOMD parameters). These spectra were reported elsewhere but did not include the MOMD simulations.[17]

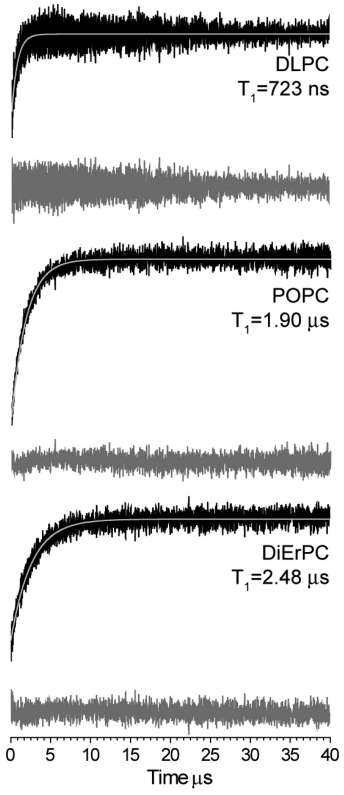

Figure 8. Saturation recovery data (black traces) for 156R1 reconstituted into DLPC (top), POPC (middle), and DiErPC (bottom) bilayers. Each signal could be fit with a single-exponential recovery function (white trace), and the T_1 values are given. The residual to the fit is colored gray. The first ~100 data points representing the microwave defense pulse were omitted from the fits and figures.

the intrinsic spin–lattice relaxation times of the individual motional modes.

The lower limit on the rate of exchange between the two motional modes of T156R1 could be estimated from the individual values of T_1^A and T_1^B. The MOMD fits (Table 2) indicate that the fast dynamic mode remains relatively unchanged with membrane thickness. If it is assumed that the T_1 relaxation time for the fast component remains constant, then the value of T_1^A from the DLPC saturation recovery data can be taken to be that of the fast component in each spectrum, and T_1^B can be estimated using the MOMD populations of each component (the measured saturation recovery signal should be a linear combination of T_1^A and T_1^B; e.g., for POPC, 0.74 × 723 ns + 0.26 × T_1^B = 1.90 μs). Using this approach, the saturation recovery data indicate that in POPC bilayers the exchange rate is faster than 596 kHz and in DiErPC bilayers the exchange rate is faster than 557 kHz. These correspond to interconversion times of 1.68 and 1.80 μs, respectively. Because most conformational exchange occurs no faster than tens of microseconds,[35] the two spectral components in T156R1 are likely the result of label rotameric exchange.

As indicated above, a likely alternate configuration for T156R1 is the {t,t} rotamer. Moreover, it is likely that the slow component in the EPR spectrum results from the interaction of the label in this rotamer with the hydrophobic surface of the protein. Dioxane has been used to probe weak interactions between R1 and protein surfaces,[12] and it might be expected to alter T156R1 line shapes by modulating the interaction of the label with the protein surface. Shown in Figure 9 are EPR

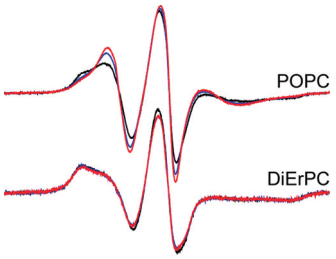

Figure 9. Effect of dioxane on the EPR spectrum of BtuB 156R1. Spectra are shown in the absence of dioxane (black) and in the presence of 5% (v/v) (blue) and 10% (red) dioxane. In POPC bilayers, dioxane increases the population of the fast component, consistent with the proposal that the slow label conformer results from an interaction of the label with a hydrophobic pocket on the protein surface. In DiErPC bilayers, dioxane does not affect the rotameric equilibrium, presumably because this interaction is much stronger in thicker lipid bilayers.

spectra that result from titration of dioxane into BtuB T156R1 reconstituted into bilayers. For the POPC sample, dioxane increases the population of the 156R1 fast component as well as the correlation time of the slow component (MOMD fits not shown), suggesting that dioxane competes with the spin-label for the surface of the protein and weakens the interaction between R1 and the protein surface. Interestingly, in DiErPC bilayers, dioxane has no effect at concentrations up to 10% (v/v) but solubilizes the liposomes above this threshold, as reported previously.[36] It is not clear why the behavior in DiErPC is different, but this result could indicate that the side chain R1 interacts more strongly with the protein surface in these membranes and is not effectively displaced by dioxane.

dx.doi.org/10.1021/bi200971x | Biochemistry 2011, 50, 8792–8803

Structural Model of W371R1 from X-ray Crystallography. W371R1 is located deep in the membrane bilayer and exhibits an EPR spectrum near the rigid limit (Figure 1d); however, its nearest-neighbor residues consist of a glycine, an alanine, and two threonines. To determine why R1 is highly immobilized at this site, the structure of 371R1 was determined at 90 K. The crystals diffracted to 2.3 Å, and the resulting structure was refined to an R_{free} of 24.98%; the complete data collection and refinement statistics are listed in Table 1. As seen for 156R1, electron density for the entire R1 side chain is resolved (Figure 10), and χ_1 and χ_2 are in a {p,p} rotamer

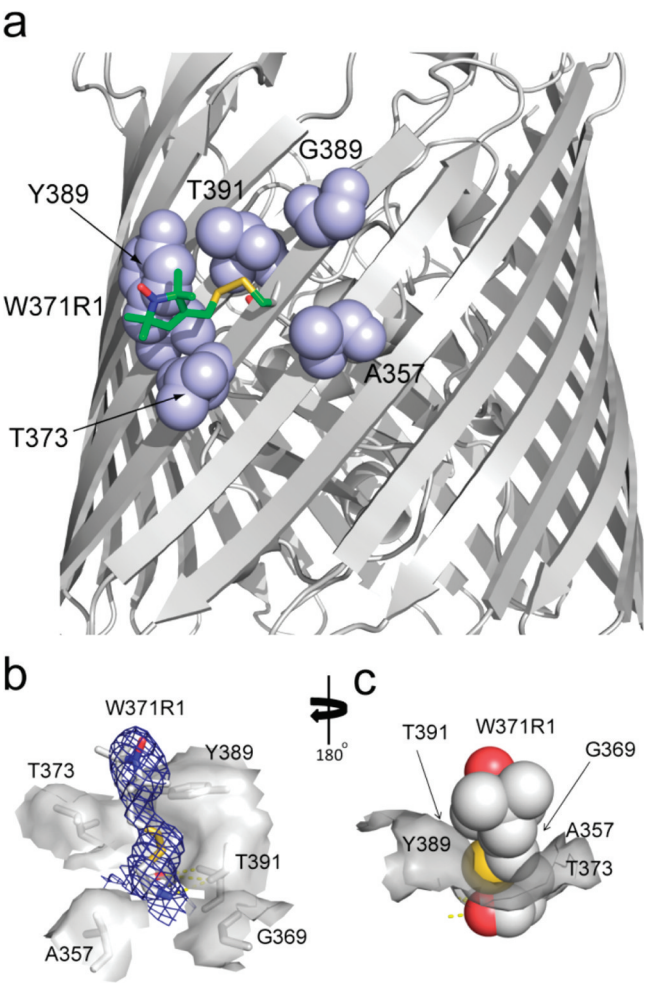

Figure 10. (a) X-ray crystal structure (90 K) of BtuB W371R (PDB entry 3RGN) determined at 2.3 Å showing the R1 side chain (as sticks) and the positions of the nearest-neighbor residues in a Corey, Pauling Koltun rendering. (b and c) Alternate views of the site around W371R1, with the van der Waals surface colored gray. W371R1 sits in a pocket formed by residues T373 and Y389. In panel b, the $2F_o - F_c$ electron density is shown as blue mesh contoured at 1σ. Data collection and refinement statistics are listed in Table 1.

(Table 2). This R1 rotamer has been reported only once in the literature,[21] for a label in a sterically constrained environment in tertiary contact.

The W371R1 mutation does not affect BtuB structure; the all-atom pairwise rmsd compared to the wild-type apo structure[24] is 0.22 Å, and the neighboring side chain rotamers are all unperturbed. It should be noted that residue 371 is near a BtuB crystal contact site on a neighboring β-strand; however, W371R1 does not contact the BtuB symmetry partner, and the rotameric state of R1 does not appear to be affected by this proximity. As seen for T156R1, the S_δ–HC_α stabilizing interaction found at many spin-labeled α-helical sites is absent (d = 4.5 Å). Instead, 371R1 may be stabilized internally by S_δ–N_{i+1} (d = 3.6 Å) and S_δ–O═C (3.0 Å) interactions similar to that of the 156R1 side chain. The spin-label sits in a pocket formed by Y389 and T373. A methyl group on the nitroxide ring interacts with Y389 C_ε2-H (d_{H-H} = 2.2 Å); the R1 S_δ atom interacts with Y389 C_δ2-H and C_ε2-H (d_{S-H} = 3.2 Å), and the R1 C_ε-H group may interact with O_γ of T373 (d_{H-O} = 3.0 Å). In other BtuB structures, W371 sits in this same pocket on the protein surface. Because of the increased level of strand twist, there is limited interstrand hydrogen bonding between the N-terminal end of strand 12 and the C-terminal end of strand 13. Nevertheless, this does not result in any measurable increase in backbone dynamics because the 371R1 line shape is near the rigid limit. Although a considerable amount of strand tilt on β-strand 13 points the side chains toward 371R1, the increased level of strand twist places the C_α atom of the HB neighbor T391 ~2 Å below the C_α atom of 371R1, decreasing the chance of a strong interaction between 371R1 and its hydrogen-bonded neighbor regardless of residue identity.

The configuration of W371R1 in this structural model is consistent with the broad spectrum that is obtained at room temperature. This model suggests that R1 at this deeply buried hydrophobic site interacts with a pocket on the protein surface formed by neighboring side chains. This site does not present a sterically restrictive environment to the R1 side chain, and the interaction of R1 with this pocket must be sufficiently strong to immobilize the nitroxide on the nanosecond time scale. Unfortunately, we were unable to obtain a room-temperature crystalline EPR spectrum, because there were not enough crystals to produce a spectrum with a reasonable signal-to-noise ratio. Unlike the label at site 156, W371R1 is not sensitive to hydrocarbon thickness, perhaps because it is more deeply buried in the bilayer (data not shown).

EPR Spectra of G170R1 Are Insensitive to Local Side Chain Substitutions. G170R1 is located at a site buried in the membrane interior that also yields a rigid-limit EPR spectrum; however, it is surrounded by a more sterically restrained environment than W371R1. At this site, we mutated surrounding residues to alanine to determine whether specific side chains interactions with G170R1 might be important for immobilization of the spin-label. The resulting EPR line shapes are shown in Figure 11. The results indicate that the motion of G170R1 is only very weakly dependent on the identity of nearest-neighbor residues. Tyrosine, a residue that has been shown to interact with and stabilize the nitroxide ring,[13] is the i + 2 neighbor of G170. However, exchanging the tyrosine at residue 172 with an alanine did not significantly affect EPR line shape; in fact, there was a minor decrease in the peak-to-peak amplitude, indicating additional immobilization of R1. The peak-to-peak amplitude of the central line also slightly decreases when residue i − 2 is mutated to alanine, indicating a further immobilization of the spin-label when the local steric environment decreases on the same β-strand as R1. For all the mutants, small changes in g anisotropy can be seen in the central line, which may reflect changes in local side chain polarity. Furthermore, in contrast to the spectra from 156R1, the EPR line shape from G170R1 is not dependent upon lipid composition. These results suggest that G170R1 is not being immobilized by specific interactions made with neighboring

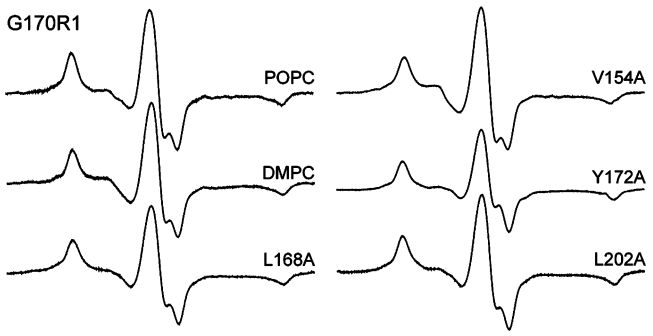

Figure 11. EPR spectra of BtuB G170R1 reconstituted into POPC and DMPC bilayers and spectra from four mutations surrounding G170R1, reconstituted into POPC bilayers, where nearest-neighbor residues were mutated to alanine. These spectra include those from mutations to the $i \pm 2$ residues (Y172 and L168) and the hydrogen-bonded (V154) and non-hydrogen-bonded (L202) neighbors. All spectra are 100 G scans.

residues; in other words, at this deeply buried site, R1 can form strong interactions with the protein surface irrespective of the identity of the neighboring side chain.

DISCUSSION

At aqueous solvent-exposed helical sites, the spin-labeled side chain R1 does not make strong interactions with neighboring residues;[10,14] however, the disulfide linkage interacts with the protein backbone, and differences in EPR spectra are dominated by differences in backbone dynamics.[37] On β-sheet proteins facing an aqueous environment, EPR spectroscopy indicates that the side chain R1 interacts strongly with neighboring residues and the motion of the label is strongly modulated by the identity of the HB and NHB neighbors.[16] For labels in a hydrophobic environment, such as the surface of a membrane protein, the work presented here indicates that the R1 nitroxide ring makes interactions with hydrophobic pockets on the protein surface, and that the label–protein interaction is sensitive to the solvation environment.

Recent work on the structures of R1 at helix surface sites in LeuT indicates that R1 is more likely to interact with the protein surface at protein–hydrocarbon interfaces than at protein–aqueous interfaces.[15] The work presented here is consistent with this result and with the general finding that side chain rotamers that face the hydrocarbon in transmembrane proteins (either α-helical or β-barrel) are different versus those in soluble proteins.[38] The data presented here indicate that T156R1, W371R1, and G170R1 interact with hydrophobic pockets formed by side chains on the β-barrel surface of BtuB. In the case of W371R1, the room-temperature EPR spectrum is highly immobilized, even though the site is not sterically restrictive. The crystal structure of BtuB W371R1 indicates that this immobilization is due to the interaction of the nitroxide ring with a pocket formed by Y389 and T373. A common configuration for R1 at helical surface sites is the {m,m} or {t,p} rotamer for χ_1 and χ_2; however, at position 371, the R1 side chain is in a {p,p} rotamer, which has been observed only once at a sterically hindered site.[21] It is likely that this rotamer is being dictated by interactions of the R1 side chain with the pocket formed by Y389 and T373. The G170R1 mutagenesis data further indicate that R1 labels buried in the membrane interior are immobilized by interactions with the protein surface, and not by interactions with specific neighboring side chains. In the case of T156R1, the {t,m} conformer observed in the crystal structure projects away from the protein backbone and toward the solvent interface. The interaction of the spin-label with the protein surface at this site appears to be weaker and modulated by the solvation environment.

Several other observations support the idea that a hydrocarbon environment promotes interactions of the R1 side chain with the protein surface. As indicated above, strongly immobilized EPR spectra on the surface of BtuB arise almost exclusively from labels positioned in the membrane hydrocarbon, while multicomponent spectra appear to be more prevalent at interfacial sites. Although sites on the positively curved surface of BtuB are less sterically constrained than sites on cellular retinol binding protein (CRBP), a soluble β-sheet protein, the EPR spectra of CRBP[16] exhibit more motional averaging than those found on the hydrocarbon surface of BtuB. Interactions of R1 with the protein surface will become more important if interactions with the surrounding solvent are less favorable, and this may be the case at the protein–hydrocarbon interface. Spin-labels on BtuB were previously seen to be insensitive to the phase state of the bulk lipid,[17] which is consistent with the finding here that R1 tends to interact with the protein surface at the protein–hydrocarbon interface.

The work presented here provides an explanation for the dramatic sensitivity of the EPR spectrum at position 156 to lipid chain length. Membrane thickness modulates two rotameric states of R1 at this site, which gives rise to fast and slow components in the EPR spectrum. Why should the EPR spectrum of residue 156 be sensitive to membrane hydrocarbon thickness? Conceivably, lipid thickness modulates the local acyl chain packing at this site or alters the exposure of this site to water. Altering the polarity gradient along the protein surface has, in fact, been shown to affect side chain rotamer conformations.[38] Similar to that seen in the thinnest bilayer formed from DLPC, BtuB T156R1 in the C_8E_4 detergent system produces only a single fast component in the EPR spectrum (see Figure 4). We speculate that the local polarity or degree of water penetration at this site is much greater in the detergent or short chain lipid.

Previously, it was noted that three other outward-facing sites studied on β-strand 2 are sensitive to lipid thickness.[17] The spectra at these sites (150, 152, and 154) also result from two motional components, and lipid composition appears to modulate the populations of these components. As a result, the effects seen at position 156 are not limited to sites near the solvent interface. These lipid effects have not been observed elsewhere on the BtuB barrel at deeply buried hydrocarbon sites (strands 3, 7, 12, and 17), which suggests that this end of the BtuB barrel may be different than other regions of the protein.

The length of the β-strands in the barrel of BtuB, and other TonB-dependent transporters, is highly asymmetric around the circumference of the protein. Recent work using nitroxide depth measurements indicates that the protein–bilayer interface is also asymmetric around the circumference of BtuB, and that the region near strand 1 is highly mismatched to the hydrocarbon thickness.[19] Conceivably, this hydrophobic mismatch might alter the optimal lipid chain packing with the protein surface, create more local defects in the bilayer, and/or alter water penetration around this surface of the protein, thereby modulating the interactions of labels with the protein surface at this site. This region of BtuB (β-strands 22, 1, and 2)

also has higher crystallographic *B* factors in both the *in meso* and *in surfo* structures than other regions around the protein β-barrel.[24,39] Although the MOMD fits of spectra from T156R1 do not suggest that nanosecond backbone dynamics are directly contributing to motional averaging of the label, it is possible that slow backbone fluctuations around strand 2 are altering interactions of the label with the protein surface.

In summary, the R1 spin-labeled side chain tends to interact with the protein surface at hydrocarbon-facing sites in BtuB. In contrast to aqueous-facing sites, the mobility of R1 on the BtuB barrel and the resulting EPR spectra at these sites are influenced by the availability of binding pockets for R1 on the surface of the protein and not necessarily by steric constraints due to neighboring residues. Moreover, R1 is highly sensitive to the solvation environment, and at some sites, interactions of the label with the protein can be modulated by lipid chain length.

The R1 side chain is widely used as a probe to obtain long-range distance restraints for molecular modeling, either through measurements of paramagnetic enhancements of nuclear relaxation or through measurements of electron dipole−dipole interactions. In these cases, knowledge of the likely side chain configurations for R1 becomes an important factor in modeling the structure with the desirable resolution. The work presented here indicates that the rotamers found for R1 at aqueous-exposed sites in β-barrel membrane proteins will likely be different from those found for sites facing the membrane hydrocarbon. Even in cases where R1 is not restrained by interactions with neighboring residues, it is likely to be restrained due to interactions with the protein surface at sites located within the membrane interior.

AUTHOR INFORMATION

Corresponding Author

*Department of Chemistry, McCormick Road, University of Virginia, Charlottesville, VA 22904-4319. E-mail: cafiso@virginia.edu. Telephone: (434) 924-3067. Fax: (434) 924-3567.

Funding

This work was supported by National Institute of General Medical Sciences Grants GM 035215 to D.S.C. and 079800 to M. C. Wiener.

ACKNOWLEDGMENTS

We thank Prof. Michael C. Wiener (Department of Molecular Physiology, University of Virginia) for the use of his facilities to generate BtuB crystals and refine crystallographic data and Dr. Christian Altenbach for providing LabVIEW programs used to process and simulate EPR spectra. Use of the Advanced Photon Source was supported by the U.S. Department of Energy, Office of Science, Office of Basic Energy Sciences, under Contract DEAC02-06CH11357. Data were collected at Southeast Regional Collaborative Access Team (SER-CAT) 22-ID and 22-BM beamlines at the Advanced Photon Source, Argonne National Laboratory. Supporting institutions may be found at http://www.ser-cat.org/members.html.

ABBREVIATIONS

EPR, electron paramagnetic resonance; MTSL, methanethiosulfonate spin-label; C_8E_4, *n*-octyl tetraoxyethylene; PC, phosphatidylcholine; DLPC, dilauroylphosphatidylcholine; DMPC, dimyristoylphosphatidylcholine; MTSL, methanethiosulfonate spin-label; PDB, Protein Data Bank; POPC, palmitoyloleoylphosphatidylcholine; R1, spin-labeled side chain produced by derivatization of a cysteine with MTSL; rmsd, root-mean-square deviation; SDSL, site-directed spin-labeling.

REFERENCES

(1) Klug, C. S., and Feix, J. B. (2008) Methods and applications of site-directed spin labeling EPR spectroscopy. *Methods Cell Biol. 84*, 617−658.

(2) Jeschke, G., and Polyhach, Y. (2007) Distance measurements on spin-labelled biomacromolecules by pulsed electron paramagnetic resonance. *Phys. Chem. Chem. Phys. 9*, 1895−1910.

(3) Fanucci, G. E., and Cafiso, D. S. (2006) Recent advances and applications of site-directed spin labeling. *Curr. Opin. Struct. Biol. 16*, 644−653.

(4) Hubbell, W. L., Cafiso, D. S., and Altenbach, C. (2000) Identifying conformational changes with site-directed spin labeling. *Nat. Struct. Biol. 7*, 735−739.

(5) Hubbell, W. L., Gross, A., Langen, R., and Lietzow, M. A. (1998) Recent advances in site-directed spin labeling of proteins. *Curr. Opin. Struct. Biol. 8*, 649−656.

(6) Clore, G. M., Tang, C., and Iwahara, J. (2007) Elucidating transient macromolecular interactions using paramagnetic relaxation enhancement. *Curr. Opin. Struct. Biol. 17*, 603−616.

(7) Liang, B., Bushweller, J. H., and Tamm, L. K. (2006) Site-directed parallel spin-labeling and paramagnetic relaxation enhancement in structure determination of membrane proteins by solution NMR spectroscopy. *J. Am. Chem. Soc. 128*, 4389−4397.

(8) Columbus, L., and Hubbell, W. L. (2004) Mapping backbone dynamics in solution with site-directed spin labeling: GCN4−58 bZip free and bound to DNA. *Biochemistry 43*, 7273−7287.

(9) Columbus, L., Kalai, T., Jeko, J., Hideg, K., and Hubbell, W. L. (2001) Molecular motion of spin labeled side chains in α-helices: Analysis by variation of side chain structure. *Biochemistry 40*, 3828−3846.

(10) Fleissner, M. R., Cascio, D., and Hubbell, W. L. (2009) Structural origin of weakly ordered nitroxide motion in spin-labeled proteins. *Protein Sci. 18*, 893−908.

(11) Guo, Z., Cascio, D., Hideg, K., and Hubbell, W. L. (2008) Structural determinants of nitroxide motion in spin-labeled proteins: Solvent-exposed sites in helix B of T4 lysozyme. *Protein Sci. 17*, 228−239.

(12) Guo, Z., Cascio, D., Hideg, K., Kalai, T., and Hubbell, W. L. (2007) Structural determinants of nitroxide motion in spin-labeled proteins: Tertiary contact and solvent-inaccessible sites in helix G of T4 lysozyme. *Protein Sci. 16*, 1069−1086.

(13) Langen, R., Oh, K. J., Cascio, D., and Hubbell, W. L. (2000) Crystal structures of spin labeled T4 lysozyme mutants: Implications for the interpretation of EPR spectra in terms of structure. *Biochemistry 39*, 8396−8405.

(14) McHaourab, H. S., Lietzow, M. A., Hideg, K., and Hubbell, W. L. (1996) Motion of spin-labeled side chains in T4 lysozyme. Correlation with protein structure and dynamics. *Biochemistry 35*, 7692−7704.

(15) Kroncke, B.M., Horanyi, P. S., and Columbus, L. (2010) Structural Origins of Nitroxide Side Chain Dynamics on Membrane Protein α-Helical Sites. *Biochemistry 49*, 10045−10060.

(16) Lietzow, M. A., and Hubbell, W. L. (2004) Motion of spin label side chains in cellular retinol-binding protein: Correlation with structure and nearest-neighbor interactions in an antiparallel β-sheet. *Biochemistry 43*, 3137−3151.

(17) Xu, Q., Kim, M., Ho, K. W., Lachowicz, P., Fanucci, G. E., and Cafiso, D. S. (2008) Membrane hydrocarbon thickness modulates the dynamics of a membrane transport protein. *Biophys. J. 95*, 2849−2858.

(18) Fanucci, G. E., Cadieux, N., Piedmont, C. A., Kadner, R. J., and Cafiso, D. S. (2002) Structure and dynamics of the β-barrel of the membrane transporter BtuB by site-directed spin labeling. *Biochemistry 41*, 11543−11551.

(19) Ellena, J. F., Lackowicz, P., Mongomery, H., and Cafiso, D. S. (2011) Membrane Thickness Varies Around the Circumference of the Transmembrane Protein BtuB. *Biophys. J. 100*, 1280−1287.
(20) Chimento, D. P., Mohanty, A. K., Kadner, R. J., and Wiener, M. C. (2003) Crystallization and initial X-ray diffraction of BtuB, the integral membrane cobalamin transporter of *Escherichia coli*. *Acta Crystallogr. D59*, 509−511.
(21) Freed, D. M., Horanyi, P. S., Wiener, M. C., and Cafiso, D. S. (2010) Conformational Exchange in a Membrane Transport Protein Is Altered in Protein Crystals. *Biophys. J. 99*, 1604−1610.
(22) Otwinowski, Z., and Minor, W. (1997) Processing of X-ray diffraction data collected in oscillation mode. *Methods Enzymol. 276*, 307−326.
(23) Mccoy, A. J., Grosse-Kunstleve, R. W., Adams, P. D., Winn, M. D., Storoni, L. C., and Read, R. J. (2007) Phaser crystallographic software. *J. Appl. Crystallogr. 40*, 658−674.
(24) Chimento, D. P., Mohanty, A. K., Kadner, R. J., and Wiener, M. C. (2003) Substrate-induced transmembrane signaling in the cobalamin transporter BtuB. *Nat. Struct. Biol. 10*, 394−401.
(25) Emsley, P., and Cowtan, K. (2004) Coot: Model-building tools for molecular graphics. *Acta Crystallogr. D60*, 2126−2132.
(26) Winn, M. D., Isupov, M. N., and Murshudov, G. N. (2001) Use of TLS parameters to model anisotropic displacements in macromolecular refinement. *Acta Crystallogr. D57*, 122−133.
(27) Murshudov, G. N., Vagin, A. A., and Dodson, E. J. (1997) Refinement of macromolecular structures by the maximum-likelihood method. *Acta Crystallogr. D53*, 240−255.
(28) Adams, P. D., Grosse-Kunstleve, R. W., Hung, L. W., Ioerger, T. R., McCoy, A. J., Moriarty, N. W., Read, R. J., Sacchettini, J. C., Sauter, N. K., and Terwilliger, T. C. (2002) PHENIX: Building new software for automated crystallographic structure determination. *Acta Crystallogr. D58*, 1948−1954.
(29) Davis, I. W., Leaver-Fay, A., Chen, V. B., Block, J. N., Kapral, G. J., Wang, X., Murray, L. W., Arendall, W. B. III, Snoeyink, J., Richardson, J. S., and Richardson, D. C. (2007) MolProbity: All-atom contacts and structure validation for proteins and nucleic acids. *Nucleic Acids Res. 35*, W375−W383.
(30) Budil, D. E., Lee, S., Saxena, S., and Freed, J. H. (1996) Nonlinear-least-squares analysis of slow-motion EPR spectra in one and two dimensions using a modified Levenberg-Marquardt algorithm. *J. Magn. Reson., Ser. A 120*, 155−189.
(31) Lovell, S. C., Word, J. M., Richardson, J. S., and Richardson, D. C. (2000) The penultimate rotamer library. *Proteins 40*, 389−408.
(32) Warshaviak, D. T., Serbulea, L., Houk, K. N., and Hubbell, W. L. (2011) Conformational analysis of a nitroxide side chain in an α-helix with density functional theory. *J. Phys. Chem. B 115*, 397−405.
(33) Murzin, A. G., Lesk, A. M., and Chothia, C. (1994) Principles determining the structure of β-sheet barrels in proteins. I. A theoretical analysis. *J. Mol. Biol. 236*, 1369−1381.
(34) Bridges, M. D., Hideg, K., and Hubbell, W. L. (2010) Resolving Conformational and Rotameric Exchange in Spin-Labeled Proteins Using Saturation Recovery EPR. *Appl. Magn. Reson. 37*, 363.
(35) Henzler-Wildman, K., and Kern, D. (2007) Dynamic personalities of proteins. *Nature 450*, 964−972.
(36) Glorio-Paulet, P., and Durst, R. A. (2000) Determination of potato glycoalkaloids using a liposome immunomigration, liquid-phase competition immunoassay. *J. Agric. Food Chem. 48*, 1678−1683.
(37) Columbus, L., and Hubbell, W. L. (2002) A new spin on protein dynamics. *Trends Biochem. Sci. 27*, 288−295.
(38) Chamberlain, A. K., and Bowie, J. U. (2004) Analysis of side-chain rotamers in transmembrane proteins. *Biophys. J. 87*, 3460−3469.
(39) Cherezov, V., Yamashita, E., Liu, W., Zhalnina, M., Cramer, W. A., and Caffrey, M. (2006) In meso structure of the cobalamin transporter, BtuB, at 1.95 Å resolution. *J. Mol. Biol. 364*, 716−734.
(40) Kucerka, N., Tristram-Nagle, S., and Nagle, J. F. (2005) Structure of fully hydrated fluid phase lipid bilayers with monounsaturated chains. *J. Membr. Biol. 208*, 193−202.
(41) Lewis, B. A., and Engelman, D. M. (1983) Lipid bilayer thickness varies linearly with acyl chain length in fluid phosphatidylcholine vesicles. *J. Mol. Biol. 166*, 211−217.